Low-frequency scattering by correlated distributions of randomly oriented particles[a)]

Victor Twersky
Mathematics Department, University of Illinois, Chicago, Illinois 60680

(Received 9 September 1986; accepted for publication 27 January 1987)

Random distributions of correlated scatterers averaged over orientation are considered, corresponding to isotropic fluids of statistical mechanics particles (with volume v, number concentration ρ, and volume fraction $w = \rho v$). For minimum separation of centers small compared to wavelength and acoustic particle parameters close to the embedding medium's, the incoherent differential scattering from unit volume and the corresponding attenuation coefficient are proportional to the fluctuations (variance) in number concentration. For arbitrary convex hard particles (e.g., ovals or simple polyhedra, repulsive at contact) with shape parameter $c \geqslant 3$, the variance is expressed in terms of a quotient $S(c;w)$ of polynomials in w that has a maximum $S'_\Lambda(c)$ at $w'_\Lambda(c)$. Spheres ($c = 3$) were considered earlier. For $c > 3$, the fluctuations and S'_Λ and w'_Λ are smaller than for spheres; for $c < 3$ (which we consider formally), they are larger than for spheres. The results are interpreted by comparing leading terms with the second virial coefficients for more general statistical mechanics models. Scattering data for suspensions of discoidal red blood cells versus w under different flow conditions can be fitted adequately by $S(c;w)$ for different values of $c < 3$. The low values of c suggest weaker repulsion between deformable cells, and attractive interparticle forces mediated by flow and aggregative trends.

PACS numbers: 43.80.Cs, 43.20.Fn

INTRODUCTION

Earlier papers[1-4] analyzed the average field in random distributions of correlated scatterers corresponding to fluids of hard[5] statistical mechanics particles (with volume v, number concentration ρ, and volume fraction $w = \rho v$). The low-frequency scattering and the corresponding attenuation depend on the fluctuations (variance) in number concentration. Using the scaled particle[6] approximate equation of state E, we expressed the variance in terms of a simple quotient $S(w)$ of polynomials that vanishes at the extremes of w. For spheres[7] (as well as aligned ellipsoids), $S(w)$ has a maximum $S_\Lambda \approx 0.047$ at $w_\Lambda \approx 0.129$. Now we consider a generalization $S(c;w)$ for isotropic fluids of nonspherical particles averaged over orientation, with c as a parameter. For arbitrary convex particles (such that a line segment connecting any two points in v is wholly within v), c is determined by the volume, surface, and average over angles of the mean of the principal radii of curvature.[8-10] For such cases, Gibbons[11] applied scaled particle theory in terms of Isihara's[8] results for two different convex particles to obtain $E(c)$, which we use to construct $S(c;w)$.

Convex hard particles require $c \geqslant 3$, with $c = 3$ as the special case of spheres, and $c > 3$ as a nonsphericity parameter. For $c > 3$, we show that S_Λ and w_Λ are smaller than for spheres. We also consider $3 > c \geqslant 0$ formally, in which range they are larger: $0.047 \leqslant S_\Lambda \leqslant 0.148$ and $0.129 \leqslant w_\Lambda \leqslant 0.333$. (The Appendix analyzes E and S for $c < 0$.) The behavior of $S(c;w)$ is uniform in w for all $c \geqslant 0$, and its simplicity suggests inverting data showing a peak at $0 < w_\Lambda \leqslant 1/3$ to obtain an effective $c(w_\Lambda)$. For $c > 3$, we expect the upper bound on w to be less than for spheres (≈ 0.63).

For a hard sphere, the cocentered exclusion volume (that excludes all other sphere centers) equals $8v$. The average exclusion volume for hard (repulsive at contact) convex particles[8] is $v_e(c) = 2(c+1)v$, and for $c > 3$ the fluctuations are smaller because $v_e > 8v$ (less elbow room); this also holds for nonconvex bodies[12,13] with an effective $c > 3$. If we use the form $v_e(c)$ for $c < 3$, we may interpret the larger fluctuations in terms of an effective $v_e < 8v$ arising from additional neighbors at small separations; comparison of leading terms with the second virial coefficients[14] for nonhard particles suggests attractive weakly repulsive models.

Values of $v_e > 8v$ with effective $c > 3$ do not imply convexity; see Isihara's results[12] for nonconvex particles formed from two hard spheres. Although the work by Gibbons[11] is based on convex particles, Rigby[13] found adequate accord between $E(c)$ for the nonconvex tangent dumbbell[12] and Monte Carlo computations. Similar accord is shown between $S(c;w)$ for different values of $c < 3$ and reduced ultrasonic backscattering data[15] versus w for suspensions of discoidal red blood cells under different flow conditions (stationary or stirred, or in uniform or turbulent flow). The lower effective c values suggest weaker repulsion between the cells (flexible deformable biconcave discoids), and attractive interparticle forces mediated by flow and aggregative trends; values nearer 3 may arise from flow alignment. Although additional factors may be involved, comparisons with available data[15] indicate utility of $S(c;w)$ for other than hard convex particles.

a) Work supported in part by the Office of Naval Research and the National Science Foundation.

 0001-4966/87/051609-10$00.80

For minimum separation (b) of particle centers small compared to wavelength ($\pi 2/k$) and acoustic particle parameters close to the embedding medium's, scattering aspects are particularly simple. The fluctuation function S and the isolated particle scattering (total and differential) and absorption cross sections suffice for the coherent attenuation coefficient, and for the incoherent scattering from unit volume (except for translational and transducer factors). Although the required forms can be obtained by simplifying earlier results, key steps of direct derivations are included to facilitate applications and indicate limitations. We also consider the analogous two-dimensional problem of parallel cylinders and obtain the corresponding $S(c;w)$ by using a scaled convex disk[16] $E(c)$; these results also apply for monolayers[4] of bounded particles. The one-dimensional and the lattice gas forms of S are included for comparison. For all cases, the function E corresponds to the equation of state times v (which leads to simpler forms), but we use no special label for the normalized version.

I. SCATTERING ASPECTS

We consider a plane wave $\phi e^{-i\omega t}$,

$$\phi = e^{i\mathbf{k}\cdot\mathbf{r}}, \quad \mathbf{k}\cdot\mathbf{r} = kr\hat{\mathbf{k}}\cdot\hat{\mathbf{r}} = kr\cos\theta = kz, \tag{1}$$

incident on an acoustically penetrable obstacle of volume v with center at $r = 0$ (the phase origin taken as the center of the smallest sphere enclosing v). The corresponding solution of Helmholtz's equation exterior to v has the form $\psi = \phi + u$ with u as the scattered wave. For large kr,

$$u(\mathbf{r}) \sim f(\hat{\mathbf{r}},\hat{\mathbf{k}})(e^{ikr}/r), \tag{2}$$

where $f(\hat{\mathbf{r}},\hat{\mathbf{k}})$ is the conventionally normalized scattering amplitude for directions of incidence $\hat{\mathbf{k}}$ and observation $\hat{\mathbf{r}}$. The energy transferred via interference of ϕ and u is represented by

$$\begin{aligned} &\mathrm{Im}\, f(\hat{\mathbf{k}},\hat{\mathbf{k}})4\pi/k = \sigma_a + \sigma_s, \\ &\sigma_s = \int |f(\hat{\mathbf{r}},\hat{\mathbf{k}})|^2 d\Omega(\hat{\mathbf{r}}) = \int \sigma(\hat{\mathbf{r}},\hat{\mathbf{k}})d\Omega, \end{aligned} \tag{3}$$

where σ_a is the absorption cross section, σ_s is the scattering cross section, and $\sigma(\hat{\mathbf{r}},\hat{\mathbf{k}}) = |f(\hat{\mathbf{r}},\hat{\mathbf{k}})|^2$ is the differential scattering cross section.

The obstacle is specified by two relative acoustic parameters C' and B', such that $\eta'^2 = C'/B'$ with η' as the relative index of refraction in v. For the simplest cases, C' is the relative compressibility and $1/B'$ the relative mass density; more generally, the parameters are complex with $\mathrm{Im}\, C' > 0$ and $\mathrm{Im}\, B' < 0$ to account for absorption. For small $C' - 1$ and $B' - 1$, and largest diameter ($2a$) small compared to wavelength, we use Rayleigh's form[17]

$$f(\hat{\mathbf{r}},\hat{\mathbf{k}}) \simeq [C' - 1 - (B' - 1)\hat{\mathbf{r}}\cdot\hat{\mathbf{k}}]k^2 v/4\pi \tag{4}$$

for arbitrary shaped v. To lowest orders in k, from (3),

$$\sigma_a = (\mathrm{Im}\, C' + |\mathrm{Im}\, B'|)kv, \tag{5}$$

$$\begin{aligned} &\sigma(\hat{\mathbf{r}},\hat{\mathbf{k}}) = |C' - 1 - (B' - 1)(\hat{\mathbf{r}}\cdot\hat{\mathbf{k}})|^2 k^4 v^2/16\pi^2, \\ &\sigma_s = (|C' - 1|^2 + |B' - 1|^2/3)k^4 v^2/4\pi, \end{aligned} \tag{6}$$

where σ_s follows by integration, essentially as in Rayleigh's developments.[18]

If the center of the obstacle is at $\mathbf{r}_s$ with respect to the phase origin ($r = 0$), then we replace $u(\mathbf{r})$ by $u(\mathbf{r} - \mathbf{r}_s)e^{i\mathbf{k}\cdot\mathbf{r}_s}$. For large $r \gg r_s$, we have $|\mathbf{r} - \mathbf{r}_s| \simeq r - \hat{\mathbf{r}}\cdot\mathbf{r}_s$, and

$$u(\mathbf{r} - \mathbf{r}_s)e^{i\mathbf{k}\cdot\mathbf{r}_s} = u_s\phi_s \sim f(\hat{\mathbf{r}},\hat{\mathbf{k}})e^{ik(\hat{\mathbf{k}} - \hat{\mathbf{r}})\cdot\mathbf{r}_s}(e^{ikr}/r), \tag{7}$$

where $\phi_s = e^{i\mathbf{k}\cdot\mathbf{r}_s}$ is the phase factor introduced by the incident wave.

For a configuration of N obstacles in a volume V, the multiple scattered solution has the form[19]

$$\Psi = \phi + \sum_{s=1}^{N} U_s(\mathbf{r} - \mathbf{r}_s). \tag{8}$$

The multiple scattered contribution of the sth obstacle U_s may be expressed functionally in terms of the single scattered amplitudes of all obstacles and the configurational variables (locations, orientations, etc.). Multiplying Ψ by an appropriate probability distribution function and integrating over all variables, we write the average wave (the coherent field) as

$$\langle\Psi\rangle = \phi + \sum\langle U_s\rangle. \tag{9}$$

The difference of the average of $|\Psi|^2$ and the coherent intensity $|\langle\Psi\rangle|^2$ is the incoherent scattered intensity

$$\begin{aligned} I &= \langle|\Psi|^2\rangle - |\langle\Psi\rangle|^2 \\ &= \sum_s \langle|U_s|^2\rangle + \sum_s\Big(\sum_{t\neq s}\langle U_s U_t^*\rangle - \langle U_s\rangle\sum_t\langle U_t^*\rangle\Big). \end{aligned} \tag{10}$$

For present purposes, we need consider only I explicitly.

We replace U_s in (10) by the single scattered wave $u_s\phi_s$ with implicit averages over orientation, etc. Thus the single summation reduces to $\int d\mathbf{r}_s\,\rho$ with $\rho = N/V$ as the average number of particles in unit volume for the homogeneous cases of interest. The double summation reduces to $\rho^2\int d\mathbf{r}_s\int d\mathbf{r}_t\, g(|\mathbf{r}_s - \mathbf{r}_t|)$ with $\rho^2 g$ as the pair distribution function averaged over orientation. In terms of $\mathbf{R} = \mathbf{r}_s - \mathbf{r}_t$ for the separation of centers, we recast the integral over $\mathbf{r}_t$ as an integral over $\mathbf{R}$, and use $g(R) \sim 1$ for even moderately large R. We restrict $\mathbf{r}_s$ to a relatively small central region V_c of V, a region containing the average number $\langle n\rangle = \rho V_c$ of irradiated and detected particles, and work with the farfield form as in (7). The result

$$\begin{aligned} &I(\hat{\mathbf{r}},\hat{\mathbf{k}}) = \rho V_c |f(\hat{\mathbf{r}},\hat{\mathbf{k}})|^2 W(\hat{\mathbf{r}},\hat{\mathbf{k}})/r^2, \\ &W(\hat{\mathbf{r}},\hat{\mathbf{k}}) = 1 + \rho\int [g(R) - 1]e^{ik(\hat{\mathbf{k}} - \hat{\mathbf{r}})\cdot\mathbf{R}}\, d\mathbf{R} \end{aligned} \tag{11}$$

is a standard form for x-ray scattering by dense gases or liquids.[20] The function $W(\hat{\mathbf{r}},\hat{\mathbf{k}})$ is the statistical mechanics structure factor, and $g - 1$ is the total correlation function. For minimum separation of centers small compared to wavelength (small kb), to lowest order in k,

$$\begin{aligned} &I(\hat{\mathbf{r}},\hat{\mathbf{k}}) = \Delta(\hat{\mathbf{r}},\hat{\mathbf{k}})V_c/r^2, \\ &\Delta(\hat{r},\hat{k}) \equiv \rho\sigma(\hat{\mathbf{r}},\hat{\mathbf{k}})W, \quad W = 1 + \rho\int [g(R) - 1]d\mathbf{R}, \end{aligned} \tag{12}$$

where W is the low-frequency limit of the structure factor.

The corresponding attenuation of the coherent intensity $|\langle\Psi(z)\rangle|^2 \equiv C(z)$ for single path propagation of $\langle\Psi\rangle$ in V may be obtained by Rayleigh's procedure[18] for the ideal gas

case. Thus, from (12), the net incoherent scattering from the particles in unit volume is

$$\int \Delta(\hat{\mathbf{r}},\hat{\mathbf{k}})d\Omega = \rho W \sigma_s \equiv \Delta_s, \tag{13}$$

and the energy they absorb equals

$$\gamma = \rho\sigma_a. \tag{14}$$

The sum

$$\tau = \gamma + \Delta_s = \rho(\sigma_a + \sigma_s W) \tag{15}$$

provides the attenuation coefficient for the coherent intensity in the form $dC(z)/dz = -\tau C(z)$, from which $C(z) = e^{-\tau z}$ for $C(0) = 1$. See Ref. 2 for full development of $\langle\Psi\rangle$.

The following is not restricted to three-dimensional forms of W and the single particle scattering functions in (6). Analogs for two-dimensional cases of normal incidence on parallel cylinders are based on

$$\begin{aligned} \sigma(\hat{\mathbf{r}},\hat{\mathbf{k}}) &= C' - 1 - (B' - 1)\hat{\mathbf{r}}\cdot\hat{\mathbf{k}}\, k^{-1}v^2/8\pi, \\ \sigma_s &= (C' - 1^{-2} + B' - 1^{-2}/2)k^{-1}v^2/4, \end{aligned} \tag{16}$$

which represent cross sections per unit length with v as an area. Similarly for one-dimensional problems of normal incidence on parallel slabs,

$$\begin{aligned} \sigma(\hat{\mathbf{r}},\hat{\mathbf{k}}) &= C' - 1 - (B' - 1)\hat{\mathbf{r}}\cdot\hat{\mathbf{k}}\, k^{-2}v^2/4, \\ \sigma_s &= (C' - 1^{-2} + B' - 1^{-2})k^{-2}v^2/2, \end{aligned} \tag{17}$$

which represent cross sections per unit area with v as slab thickness; here only $\hat{\mathbf{r}} = -\hat{\mathbf{k}}$ (backscattering) and $\hat{\mathbf{r}} = \hat{\mathbf{k}}$ (forward scattering) apply. The corresponding absorption cross sections (per unit length or unit area) are given by (5) in terms of the present v's.

II. STATISTICAL ASPECTS

The differential incoherent scattering and the attenuation via scattering are governed by the form

$$\Delta = \rho W\sigma = S\sigma/v, \quad S = wW, \quad w = \rho v, \tag{18}$$

where σ is either the differential or total scattering cross section, and w is the volume fraction occupied by particles. The packing function W, determined in (12) by the integral of the correlation function $g - 1$, is proportional to the[20] variance v (the mean-square deviation) of the number n of particles in V_c,

$$v = \langle (n - \langle n\rangle)^2\rangle = \langle n^2\rangle - \langle n\rangle^2 = \langle n\rangle W. \tag{19}$$

Thus

$$S = wW = vv/V_c = (\langle n^2\rangle - \langle n\rangle^2)v/V_c, \tag{20}$$

henceforth the fluctuation function, is proportional to the mean-square fluctuation in the number of particles around the mean $\langle n\rangle = \rho V_c$.

Under appropriate conditions, a distribution of particles may be regarded as a large scale fluid. The variance v, and therefore W, can then be related to statistical thermodynamical functions by

$$\frac{v}{\langle n\rangle} = \rho KT\zeta = KT\left(\frac{\partial\rho}{\partial p}\right)_T = W, \tag{21}$$

with K as Boltzmann's constant, T as absolute temperature, ζ as isothermal compressibility, and p as fluid pressure. The final equality relates W to a derivative of the equation of state $p/KT = E/v$. Using the scaled particle[6] forms of E for hard spheres, circular cylinders, and slabs (E_i with $i = 3$, 2, and 1),

$$E_3 = \frac{w(1 + w + w^2)}{(1 - w)^3}, \quad E_2 = \frac{w}{(1 - w)^2}, \quad E_1 = \frac{w}{1 - w}, \tag{22}$$

it follows from $w = \rho v$ and $dE/dw = 1/W$ that

$$W_3 = \frac{(1 - w)^4}{(1 + 2w)^2}, \quad W_2 = \frac{(1 - w)^3}{1 + w}, \quad W_1 = (1 - w)^2. \tag{23}$$

Form E_1 is the exact Tonks' equation of state, and E_2 was rederived by[21] Wertheim and by Thiele from the Percus–Yevick integral equation for g. The result W_1 follows directly by integrating[4] the Zernicke–Prins g, and both W_1 and W_3 also follow from the Percus–Yevick equation.

The packing functions $W(w)$ decrease monotonically from unity to zero as w increases from zero to unity. However, as emphasized before,[1] the fluctuation functions $S(w) = wW(w)$ vanish at the extremes of w and have a maximum $S_\wedge(w_\wedge)$ at $w = w_\wedge$ corresponding to $dS/dw = S' = 0$ and $S'' = -|S''|$. Thus

$$S_3 = \frac{w(1 - w)^4}{(1 + 2w)^2}, \tag{24}$$

$$w_\wedge = [(73)^{1/2} - 7]/12 \approx 0.129, \quad S_\wedge \approx 0.0469;$$

$$S_2 = \frac{w(1 - w)^3}{1 + w}, \tag{25}$$

$$w_\wedge = (7^{1/2} - 2)/3 \approx 0.215, \quad S_\wedge \approx 0.0856;$$

$$S_1 = w(1 - w)^2, \quad w_\wedge = 1/3, \quad S_\wedge = 4/27 \approx 0.148. \tag{26}$$

See Fig. 1 for plots versus w. Although we may consider the full range $0 \leqslant w \leqslant 1$ for some purposes, the upper bound is physically realizable only for slabs. For spheres and cylinders we use the experimental values for densest random packing, $w_{d3} \approx 0.63$ and $w_{d2} \approx 0.84$ (corresponding to amorphous solids). By geometry, the results for spheres also apply for aligned ellipsoids, and the results for circular cylinders also apply for aligned elliptic cylinders.[4]

In addition to the above cases $i = (3,2,1)$, we also showed[3] that the symmetrical function $S = w(1 - w)$ which arose in an earlier development[22] could be derived from the scaled particle[6] E for a random lattice gas:

$$E_0 = -\ln(1 - w), \quad W_0 = 1 - w; \tag{27}$$

$$S_0 = w(1 - w), \quad w_\wedge = 1/2, \quad S_\wedge = 1/4. \tag{28}$$

Shape is not specified, and $w = 1$ is realizable for special processes and compliant particles that pack to fill all space.[1] Since S_0 is not a special case of the closed forms derived in Secs. IV and V, it still serves for less correlated contexts.[22] (See Fig. 2.)

The fluctuation function determines the behavior of Δ vs w, but the total attenuation τ involves an additional term if absorption is present. We rewrite (15) as[23]

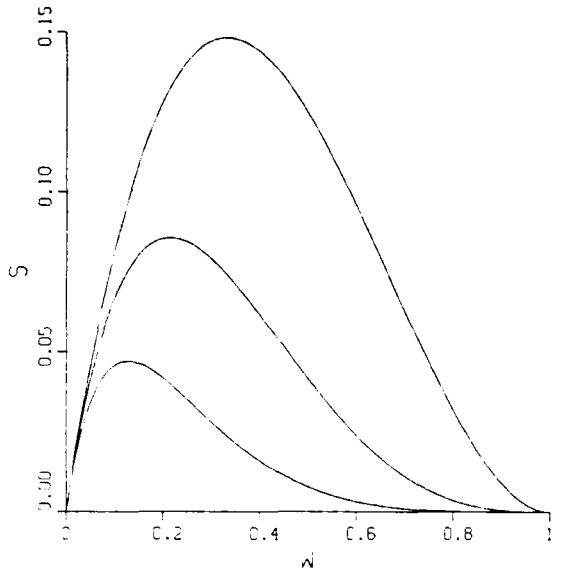

FIG. 1. Plots of the fluctuation functions S of (24)–(26) versus volume fraction w. The highest, central, and lowest curves are S_1, S_2, and S_3, respectively. (See Fig. 21 of Ref. 7 for comparison of S_3 with analogs we derived from other models.) In order to show complete curve shapes (here, as well as in all subsequent graphs versus w), the full range $0 \le w \le 1$ is displayed, but the physically realizable upper bound for w is smaller in general.

$$v\tau = \sigma_a w + \sigma_s S(w) = [\delta w + S(w)]\sigma_s, \quad \delta = \sigma_a/\sigma_s. \tag{29}$$

The occurrence of a maximum τ at $w = w_\wedge$ depends on the magnitude of δ and the requirements $w_\wedge = w_{s\wedge} < w_d$. For small δ, to first order in small terms,

$$v\tau \simeq \sigma_a w_{s\wedge} + \sigma_s S_\wedge, \quad w_\wedge \simeq w_{s\wedge} + \sigma_a/\sigma_s |S''_\wedge| > w_{s\wedge}, \tag{30}$$

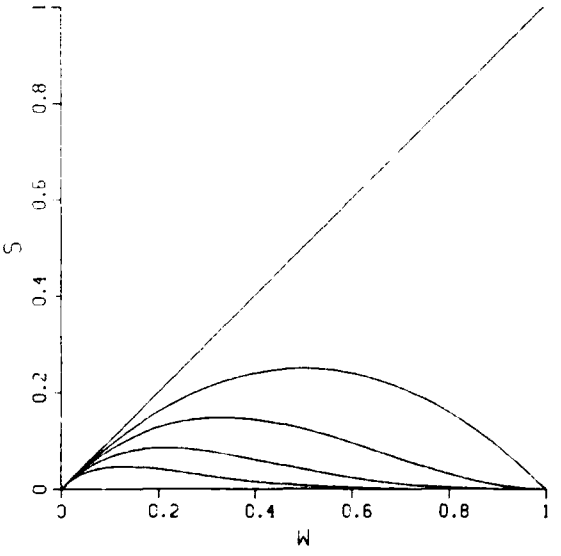

FIG. 2. Plots of the ideal gas function $S = w$ (the diagonal line), of the lattice gas S_3 (the simple parabola) of (28), and of the set shown in Fig. 1 to delineate the relative scales of the fluctuation effects and their decrease with increasing exclusion volume (decreasing elbow room).

where, corresponding to $i = (3, 2, 1, 0)$, the second derivative $|S''_\wedge| = |S''(w_\wedge)|$ approximates or equals (2.84, 2.21, 2, 2). Thus absorption shifts the maximum of τ to larger w. Because δ is small, it follows that for sparse concentrations the attenuation is dominated by scattering losses. However, since W decreases with increasing w, there is a value $w = w_x$ determined $W(w_x) = \delta$ for which absorption and scattering losses contribute equally to the attenuation and $v\tau = 2\sigma_a w_x$; for $w > w_x$, absorption dominates. On the other hand, if δ is not small, then there is in general no maximum of τ with variation of w. If $\delta > 1$, then absorption dominates the attenuation for all w.

III. SECOND VIRIAL COEFFICIENT

To facilitate derivation and interpretation of the generalizations of S given in the next sections, we consider the leading terms of the expansions of E and W in powers of ρ (virial series[14]). An ideal gas distribution corresponds to $E = \rho v$ and $W = 1$ (as well as $\nu = \langle n \rangle$ and $S = w$). The first departures from the ideal gas values are proportional to the second virial coefficient[14] B_2,

$$E_i/v_i = \rho + \rho^2 B_2 + \cdots, \quad W_i = 1 - \rho 2B_2 + \cdots, \quad 2B_2 = v_e. \tag{31}$$

with $v_e = 2^i v_i$ and $v_i = (\pi 4a^3/3, \pi a^2, 2a, v)$. The second term of W_i for $i = (3, 2, 1)$ also follows directly from (12) by using the hole approximation for the radial distribution function: $g(R) = 0$ for $R < b$, and $g(R) = 1$ for $R > b$, with $b = 2a$ as the minimum separation of particle centers.

The size of the normalized exclusion volume $v_e/v_i = 2^i = (8, 4, 2, 1)$ determines the departure from the ideal gas results. Although (31) is restricted in general to small w, comparison with S_i shows that as v_e/v_i increases, the fluctuations decrease for all w (less available space); the peak $S_\wedge$ decreases and its location $w_\wedge$ shifts to smaller values (sparser concentrations). As the ratio v_e/v_i doubles in size, the ratios of ajacent pairs of $S_{i\wedge}$ values (0.55, 0.57, 0.59) and of adjacent pairs of $w_{i\wedge}$ values (0.60, 0.645, 0.67) are of the order of half. Thus the second virial coefficient B_2 not only indicates nonideal gas behavior at small w, but also supports major trends of the maximum fluctuations $S_\wedge$ and of their locations $w_\wedge$. The generalizations of S derived in subsequent sections exhibit similar relations with B_2.

The exact second virial coefficient B_2 for an isotropic gas of arbitrary convex hard particles was derived by Isihara,[8] who determined the exclusion volume of a fixed particle by moving another in contact around it at fixed relative orientation, and then averaging over orientation. The resulting average exclusion region $v_e = 2B_2$ equals

$$v_e = 2(v + s\bar{r}) = 2v(1 + c), \quad c = \frac{s\bar{r}}{v}, \quad \bar{r} = \int (r_1 + r_2)\frac{d\Omega}{8\pi}, \tag{32}$$

with v and s as the volume and surface area of the particle, and $\bar{r}$ as the average over all angles of the mean of the particle's principal radii of curvature $(r_1 + r_2)/2$. For spheres, $c = 3$ and $v_e = 8v$ as before; for all other bounded convex particles, $c > 3$ and $v_e > 8v$. Isihara's result for v_e (and for the

average exclusion volume for two different convex particles) was obtained independently by Hadwiger,[9] and their publications and those of Kihara[10] provide additional relations and various illustrations.

The nonsphericity parameter $c > 3$ in (32) does not represent a unique shape. For example, for spheroids (both oblate and prolate), Isihara[8] obtained the single form

$$c = \frac{3}{4}\left(1 + \frac{\sin^{-1}\epsilon}{\epsilon\sqrt{1-\epsilon^2}}\right)\left[1 + \frac{1-\epsilon^2}{2\epsilon}\ln\left(\frac{1+\epsilon}{1-\epsilon}\right)\right], \qquad \epsilon^2 = 1 - \left(\frac{a'}{a}\right)^2, \tag{33}$$

with a and a' as the largest and smallest semidiameters. Thus for the same value of a'/a, both the oblate and the prolate shapes give the same value for c (corresponding essentially to an interchange of the forms s and $\bar{r}$, and using the appropriate v's). For near spheres, $a \approx a'$, and[8,10]

$$c \simeq 3 + 4(\epsilon^4 + \epsilon^6)/15. \tag{34}$$

For near disks and near needles, $a \gg a'$, and

$$c \sim 3/4 + \pi 3a/a'8 \tag{35}$$

is within 4% of (33) for $a/a' \gtrsim 3$. In this range, c increases linearly with a/a', in accord with Isihara's almost linear curve based on (33). From the complete form (33), we have

$$a/a' = (6,5,4,3,2,1.5), \qquad c \simeq (7.65,6.55,5.48,4.45,3.54,3.18), \tag{36}$$

where c decreases to the sphere value 3 for $a/a' = 1$.

For nonsmooth convex particles, from Hadwiger's[9] values (of v, s, and $\bar{r}$) for the regular polyhedra of j faces, we construct

$$j = (4,6,8,12,20), \quad c \simeq (6.7,4.5,4.32,3.56,3.45). \tag{37}$$

The largest c corresponds to tetrahedra; the progression through cubes, octahedra, dodecahedra, ends with icosahedra with c only 15% larger than for spheres.

It is clear that the value of the nonsphericity parameter for any particular polyhedron can be matched by that for a spheroid pair. Thus the tetrahedron value $c \simeq 6.7$ corresponds to spheroids with $a/a' \simeq 5.14$; the markedly jagged polyhedron is equivalent to a markedly flattened or elongated spheroid, and all three shapes yield $v_e/v \simeq 15.4$, about twice the value for spheres. [The closed form S of the next section shows that the corresponding values of $S_\wedge$ and $w_\wedge$ are of the order of half the sphere values, as may be inferred from the discussion following (31).] This aspect is stressed to indicate the limitations of c as a shape parameter; we may invert data in order to obtain c from measurements of B_2 for particles having the same volume v, but more than c is required to determine particle shape. For that matter, an effective $c > 3$ isolated by measurements need not correspond to a convex particle (or to a hard particle).

Existing results for B_2 for other than hard convex particles,[12–14] can be written formally as

$$B_2 = v_e/2 = v(c+1) \tag{38}$$

to obtain associated values of v_e and c. Although $c = s\bar{r}/v \geqslant 3$ is an exact relation for convex hard particles, an effective $c > 3$ in (38) does not imply convexity. In particular, Isihara[12] obtained the exact B_2 for the infinite set of nonconvex hard particles (dumbbells) formed from two identical spheres for all values of the center separation $b > 0$. (Only the degenerate case $b = 0$ for a single sphere corresponds to a convex particle, $c = 3$.) From his results,[12] we write

$$b/a = (0,1,2,3,4,\infty), \quad c = (3,3.329,4.444,6.031,6.8,7), \qquad b/a \geqslant 4, \quad c = 7 - 16(a/b)^2/5. \tag{39}$$

The parameter c increases smoothly from the lower bound 3 to the upper bound 7 (for which each dumbbell reduces to two independent spheres).

We can obtain effective values $c < 3$ (as well as $c > 3$) from (38) by comparison with forms of B_2 for more general models than hard particles. Although hard particles exert no forces on each other except repulsion at contact (pair potential infinite for $R \leqslant b$, and zero for $R > b$), other statistical mechanics models[14] include attractive forces for small separation (square well potential, negative for $b < R \leqslant Ab$), as well as longer range weaker repulsion and smoother attraction (Lennard–Jones potential, etc.). Analogs for the present development can be based on the integral in (12) with $g(R)$ independent of ρ. In particular, the square well potential corresponds to supplementing the hole approximation, discussed after (31), with $g(R) - 1 = \Gamma$ for $b < R < Ab$ (representing additional neighbors at small separation) to construct

$$2B_2 = 2^i v_i\left[1 - (A^i - 1)\Gamma_i\right], \quad i = (3,2,1). \tag{40}$$

For $\Gamma_i = 0$, we have $2^i v_i$ as before; we may also obtain the lattice gas result by using $A = 2$ and $\Gamma_i = 1/2^i$. For spheres, from (40) and (38),

$$2B_2 = 8v[1 - (A^3 - 1)\Gamma] = 2v(1+c), \qquad c = 3 - 4(A^3 - 1)\Gamma, \tag{41}$$

so that, e.g., if $A = 2$, then $c = (2,1,0)$ corresponds to $28\Gamma = (1,2,3)$, etc. The size of Γ can be related to an effective interparticle attractive potential, and the size of A to the range over which it acts. (Changing the sign of Γ yields $c > 3$ corresponding to fewer neighbors and repulsion for $b < R \leqslant Ab$.) Equation (41) serves for interpretation, but no closed form of S is available for this model.

For two-dimensional hard convex particles,[16] we write

$$v_e = 2v + s\bar{r} = v(2+c), \quad c = s\bar{r}/v = s^2/2\pi v, \qquad s = \int r_1\, d\theta = 2\pi\bar{r}, \tag{42}$$

with v as the cross-sectional area (or volume per unit length), s as the length of the perimeter, and $\bar{r}$ as the average of the radius of curvature (r_1). For circles, $c = 2$ and $v_e = 4v$; for all other two-dimensional convex hard figures, $c > 2$ and $v_e > 4v$. As before, a particular value of c does not represent a unique shape.

For ellipses,

$$c = (8a/a'\pi^2)\mathcal{E}^2, \quad \mathcal{E} = \int_0^{\pi/2}(1 - \epsilon^2\sin^2\theta)^{1/2}\, d\theta, \tag{43}$$

with $\mathcal{E}$ as the complete elliptic integral of the second kind. For near circles,

$$c \simeq (2a/a')(1 - \epsilon^2/2 - \epsilon^4/32), \tag{44}$$

and, for near strips,

$$c \approx (8a/a'\pi^2)\{1 + [\ln(4a/a') - 1](a'/a)^2\}, \quad a \gg a'. \quad (45)$$

From (43), the values for a set of ellipses

$$\begin{aligned} &a/a' = (6,5,4,3,2,1.5), \\ &c \approx (5.24,4.47,3.73,3.07,2.38,2.13), \end{aligned} \quad (46)$$

decrease to the circle value $c = 2$ for $a/a' = 1$.

For nonsmooth shapes, we consider j-sided regular polygons in terms of

$$c = (2j/\pi)\tan(\pi/j), \quad (47)$$

and obtain

$$\begin{aligned} &j = (3,4,5,6,8,12), \\ &c \approx (3.31,2.55,2.31,2.2,2.11,2.05). \end{aligned} \quad (48)$$

The triangle value $c \approx 3.3$ also arises for the ellipse with $a/a' \approx 3.45$; the corresponding $v_e/v \approx 5.3$ is about 33% larger than for circles.

From (38) and (40), the two-dimensional square well analog of (41) is

$$\begin{aligned} &2B_2 = 4v[1 - (A^2 - 1)\Gamma] = v(2 + c), \\ &c = 2 - 4(A^2 - 1)\Gamma \end{aligned} \quad (49)$$

so that, e.g., if $A = 2$, then $c = (1,0)$ corresponds to $12\Gamma = (1,2)$, etc.

IV. GENERALIZED THREE-DIMENSIONAL S

Gibbons[11] applied scaled particle theory[6] in terms of Isihara's result[8] for the average exclusion volume for two different particles to obtain

$$E = w[1 + w(c - 2) + w^2(1 - c + c^2/3)]/(1 - w)^3. \quad (50)$$

From $dE/dw = E' = 1/W$, we construct

$$S(c;w) = wW(c;w) = \frac{w(1 - w)^4}{[1 + (c - 1)w]^2}. \quad (51)$$

The present E and S correspond to convex hard particles if $c \geq 3$ as in (32), and reduce to the sphere results E_3 and S_3 for $c = 3$. To $O(w^2)$ we obtain (31) in terms of (32). At $w = 1/2$,

$$S(c;1/2) = 1/8(c + 1)^2 = (v/v_e)^2/2 \quad (52)$$

exhibits the direct dependence on the normalized exclusion volume.

The fluctuation function $S(c;w)$ is stationary if

$$3(c - 1)w^2 + (4 + c)w - 1 = 0 \quad (53)$$

corresponding to $dS/dw = S' = 0$, and has a maximum $S(c;w_\wedge)$ at

$$\begin{aligned} w_\wedge(c) &= \frac{(4 + 20c + c^2)^{1/2} - (4 + c)}{6(c - 1)} \\ &= \frac{2}{4 + c + (4 + 20c + c^2)^{1/2}}. \end{aligned} \quad (54)$$

From (53) we also have

$$c = 1 + (1 - 5w_\wedge)/w_\wedge(1 + 3w_\wedge) \quad (55)$$

and eliminate c from $S(c;w_\wedge) = S_\wedge$ to express the maximum

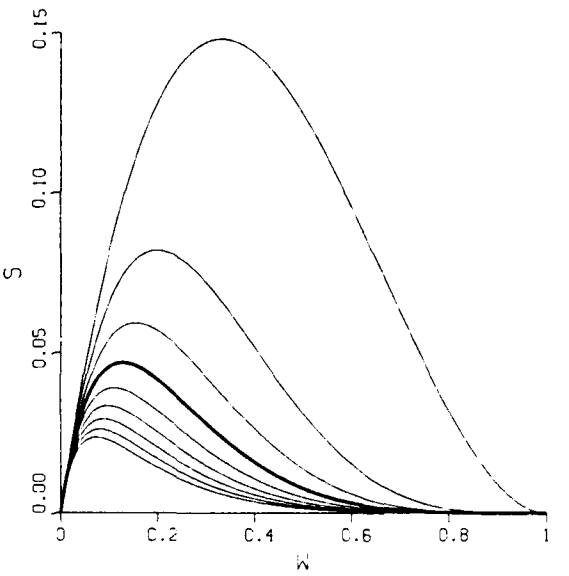

FIG. 3. Plots of the generalized three-dimensional fluctuation function $S(c;w)$ of (51) with the parameter c ranging from 0 (the highest curve) to 8 (the lowest) in steps of 1. The darker curve ($c = 3$) is the same as S_3 for hard spheres (or aligned ellipsoids); the lower curves ($c > 3$) apply for (59), and the higher curves ($c < 3$) for (60) with the highest ($c = 0$) as S_1. The maxima (the peaks $S_\wedge$) and their locations ($w_\wedge$) on the w scale are plotted in Figs. 4–6.

$$S_\wedge = w_\wedge(1 - w_\wedge)^2(1 - 3w_\wedge)^2/4 \quad (56)$$

solely in terms of its location on the volume fraction axis. We include

$$\begin{aligned} S''_\wedge &= \left.\frac{d^2S(c;w)}{dw^2}\right|_{w = w_\wedge} \\ &= -\frac{(1 - w_\wedge)^3[5 + (c - 1)(1 + 6w_\wedge)]}{[1 + (c - 1)w_\wedge]^3} \\ &= -\frac{(1 + 3w_\wedge)^2(1 + 6w_\wedge - 15w_\wedge^2)}{8w_\wedge} \end{aligned} \quad (57)$$

to facilitate applications of (30). See Figs. 3–6 for plots of all key aspects of (51)–(56).

We can apply the above to all convex hard particles, including the spheroids and polyhedra considered in (36) and (37), subject only to the restrictions of the scaled particle development. For example, for spheroids with $a/a' = 4$,

$$c \approx 5.478, \quad w_\wedge \approx 0.0932, \quad S_\wedge \approx 0.0314, \quad S''_\wedge \approx -3.14. \quad (58)$$

The maximum for spheres as in (24) is about 50% larger and occurs at a packing fraction about 38% larger; the present $-S''_\wedge$ is about 10% larger than the sphere value 2.84. As indicated in Sec. III, the differences arise from the larger size of the exclusion volume for spheroids averaged over orientation: The present $v_e/v \approx 13$ is about 62% larger than 8 for spheres, and there is less room for fluctuations. As mentioned after (26), the sphere form S_3 also holds for aligned ellipsoids; thus the above also serves for comparisons of aligned and randomly oriented spheroids.

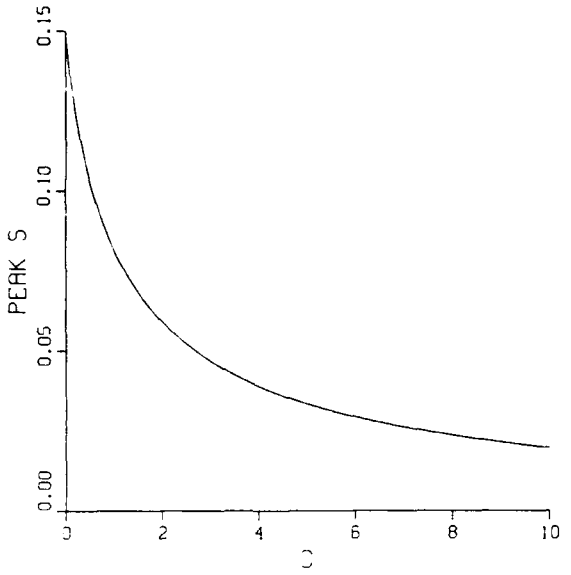

FIG. 4. Peak $S_\wedge$ vs c, based on (51) in terms of (54), corresponding to Fig. 3.

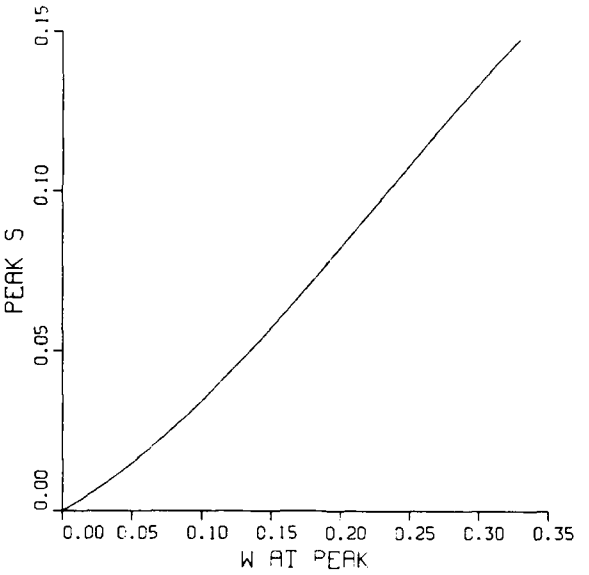

FIG. 6. Peak $S_\wedge$ vs $w_\wedge$ (with c implicit), based on (56), corresponding to Fig. 3.

Although $S(c;w)$ has the same value for both the oblate $(4, 4, 1)a'$ and prolate $(4, 1, 1)a'$ cases for given w, the prolate corresponds to four times as many particles in unit volume; for the same packing fraction, both $\langle n\rangle = \rho V_c$ (the average number in the central region V_c) and the variance $v = \langle n\rangle W = SV_c/v$ are four times larger for the prolate case. However, the normalized scattering cross sections $\Delta = S\sigma/v \propto Sv$ (and particle volumes) are four times larger for the oblate case. For special processes, the present isotropic results may be restricted to moderate values of w; with increasing packing the particles may impede each others rotational freedom, and transitions to aligned distributions may arise. For such processes involving hard ellipsoids, although we expect $S(c;w)$ and $S_3(w)$ to suffice for small and large w, respectively, the transition region need not be uniform and could entail a phase change. [For spheroids averaged over orientation within acoustically transparent spheres[3] of radius $4a'$ and volume v_3, we have $\Delta = S_3(w_\wedge)\sigma/v_3 \propto S_3 v^2/v_3$, so that the scattering is sixteen times larger for the oblate than for the prolate case. The present scattering maxima $\Delta_{\wedge,O}$ and $\Delta_{\wedge,P}$ are about 2.68 and 10.7 times larger than the sphere constrained analogs, and occur at $w_\wedge$ about 72% of the sphere value.]

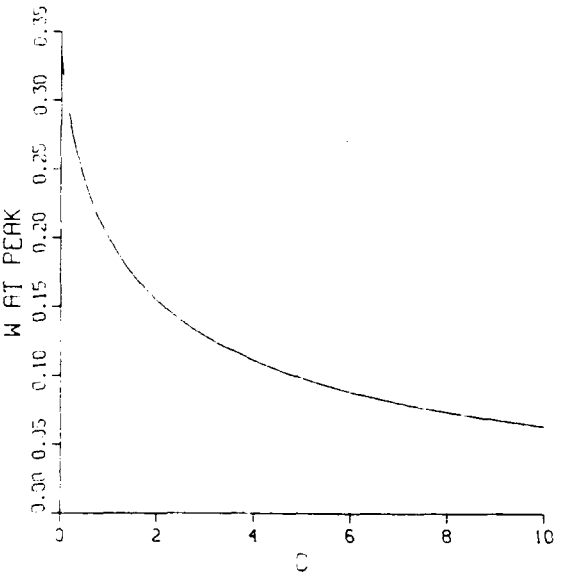

FIG. 5. Peak location $w_\wedge$ vs c, based on (54), corresponding to Fig. 3.

Although the derivation of E and S as in (50) and (51) is based on convex hard particles, the simplicity of the results suggests heuristic applications to other cases for which no closed forms in w are available. Rigby[13] used E of (50) and Isihara's[12] value for the nonconvex contact dumbbell $(b = 2a)$ with equivalent c as in (39), and reported satisfactory accord with Monte Carlo computations. Similar accord is shown between S of (51) for different values of $c \lesssim 3$ and backscattering data[15] for suspensions of particles under different flow conditions. We therefore consider $S(c;w)$ formally for all $c \geqslant 0$: In this range, S is nonsingular for all w, and has a maximum $S_\wedge \leqslant 4/27$ corresponding to $w_\wedge \leqslant 1/3$ as in (54)–(57). The bounds are attained for $c = 0$, which reproduces S_1 of (26). (The range $c < 0$ is analyzed in the Appendix.)

To display the dependence of $w_\wedge$ and $S_\wedge$ on c, we include two sets of examples, one for $c \geqslant 3$, and the other for $3 > c \geqslant 0$. Thus, covering the illustrations in (36) and (37), and including (39) formally,

$$\begin{aligned} &c = (8,7,6,5,4,3), \\ &100w_\wedge \simeq (7.38,8.03,8.83,9.82,11.1,12.9), \\ &100S_\wedge \simeq (2.36,2.62,2.94,3.35,3.9,4.69), \end{aligned} \tag{59}$$

where the final entries correspond to S_3. The second set is formal, with interpretations suggested by (41):

$$c = (2.5,2,1.5,1,0.5,0),$$
$$100w_\Lambda \approx (14,15.5,17.4,20,24.2,3.33), \quad (60)$$
$$100S_\Lambda \approx (5.23,5.92,6.9,8.2,10.3,14.8),$$

where the final entries correspond to S_1. The essential aspects of the two sets, and of the general form $S(c;w)$ of (51), change uniformly with c in the range $c \geqslant 0$.

For very large c, we have $w_\Lambda \sim 1/(c+7)$. The generalization

$$w_\Lambda \sim [4 + c + 3(c-1)/(4+c)]^{-1} \quad (61)$$

is within 2% of (54) for $c \geqslant 1$. At $c = 1$, we obtain a simple polynomial for S,

$$c = 1, \quad w_\Lambda = 0.2, \quad S_\Lambda = 0.082, \quad S = w(1-w)^4. \quad (62)$$

For c near 0,

$$w_\Lambda \approx (1 - c + 2c^2)/3, \quad (63)$$

and S reduces to the simple polynomial S_1 of (26) at $c = 0$.

V. GENERALIZED TWO-DIMENSIONAL S

Boublik[16] applied scaled particle theory[6] in terms of results for two different hard convex disks to obtain

$$E = \frac{w[1 + w(c-2)/2]}{(1-w)^2}. \quad (64)$$

From $E' = 1/W$, we construct

$$S(c;w) = wW(c;w) = \frac{w(1-w)^2}{1 + (c-1)w}. \quad (65)$$

The present E and S correspond to convex hard figures if $c > 2$ as in (42), and reduce to the circle results E_2 and S_2 for $c = 2$. To $O(w^2)$ we obtain (31) in terms of (42). At $w = 1/3$,

$$S(c;1/3) = 8/27(2 + c) = 8v/v_2 27 \quad (66)$$

exhibits the direct dependence on the exclusion region.

The fluctuation function is stationary ($S' = 0$) if

$$3(c-1)w^2 + 4w - 1 = 0 \quad (67)$$

and has a maximum S_Λ at

$$w_\Lambda(c) = \frac{(1+3c)^{1/2} - 2}{3(c-1)} = \frac{1}{2 + (1+3c)^{1/2}}. \quad (68)$$

Using

$$c = 1 + (1 - 4w_\Lambda)/3w_\Lambda \quad (69)$$

we eliminate c from $S_\Lambda = S(c;w_\Lambda)$ to obtain

$$S_\Lambda = 3w_\Lambda^2(1-w_\Lambda)^2. \quad (70)$$

The corresponding second derivative

$$S'' = -(1-w_\Lambda)^2[4 + 6(c-1)w_\Lambda]/$$
$$[1 + (c-1)w_\Lambda] = -18w_\Lambda(1-2w_\Lambda) \quad (71)$$

is required for (30). See Figs. 7–10 for plots of all key aspects of (65)–(70).

We can apply the above to any of the cases in (46) and (48), e.g., for elliptic cylinders with $a/a' = 4$,

$$c \approx 3.723, \quad w_\Lambda \approx 0.182, \quad S_\Lambda \approx 0.0666, \quad S'' \approx -2.084. \quad (72)$$

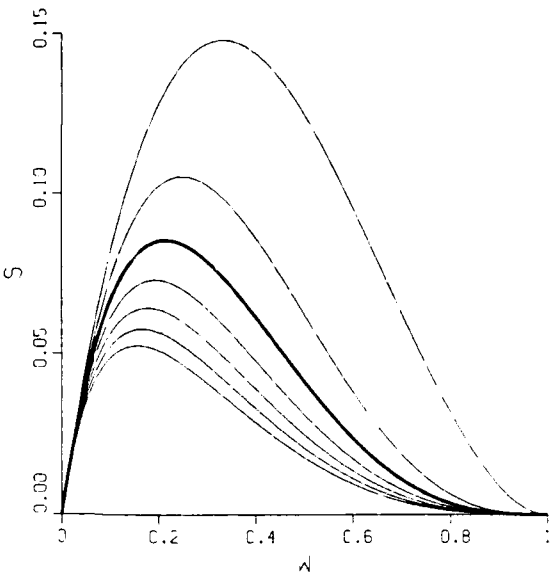

FIG. 7. The generalized two-dimensional fluctuation function $S(c;w)$ of (65) with the parameter c ranging from 0 (the highest curve) to 6 (the lowest) in steps of 1. The darker curve ($c = 2$) is the same as S_2 for hard circular cylinders (or aligned elliptic cylinders); the lower curves ($c > 2$) apply for (73), and the higher curves ($c < 2$) for (74) with the highest ($c = 0$) as S_1.

The maximum for circles (or aligned ellipses[4]) as in (25) is about 29% larger and occurs at a packing fraction about 18% larger. [For the constrained average over orientation within acoustically transparent circles[3] of radius $4a'$ and volume v_2, we use S_2 of (25) and $\Delta = S_2\sigma/v_2 \propto S_2(w_2)v^2/v_2$ with $v_2 = 4v$. The present scattering maximum $\Delta_\Lambda = S_\Lambda\sigma/v$ is about 3.1 times larger than for the circle constrained maximum, and occurs at w_Λ about 85% of the circle value.]

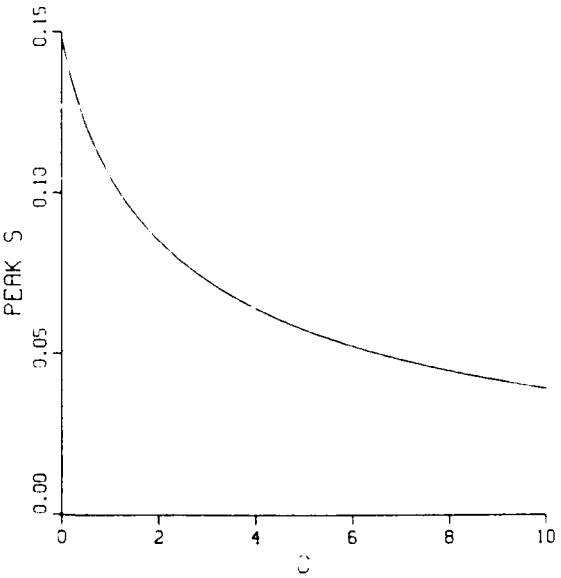

FIG. 8. Peak S_Λ vs c, based on (65) in terms of (68), corresponding to Fig. 7.

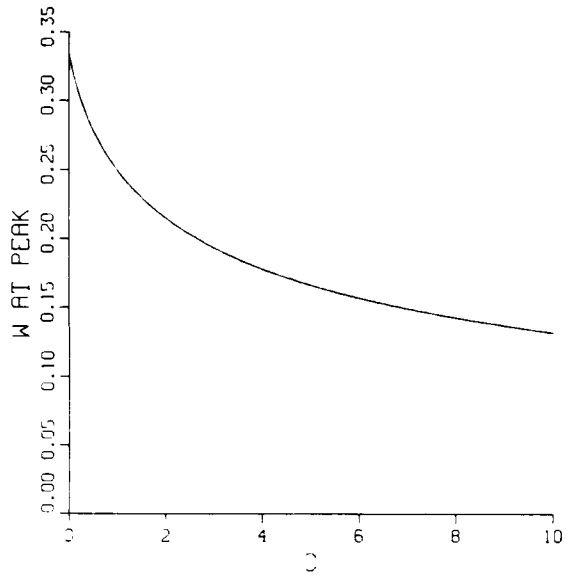

FIG. 9. Peak location $w_\wedge$ vs c, based on (68), corresponding to Fig. 7.

We proceed as for (51) and consider (65) for all $c \geqslant 0$. Thus, covering the illustrations in (46) and (48), and more generally on a formal basis for $c > 2$,

$$c = (7,6,5,4,3,2),$$
$$100w_\wedge \approx (1.49,\ 15.7,\ 16.7,\ 17.8,\ 19.4,\ 21.5), \tag{73}$$
$$100S_\wedge \approx (4.85,\ 5.27,\ 5.79,\ 6.44,\ 7.32,\ 8.56),$$

where the final entries correspond to S_2. For $2 > c \geqslant 0$, formally, with interpretations suggested by (49),

$$c = (1.5,\ 1,\ 0.75,\ 0.5,\ 0.25,\ 0),$$
$$100w_\wedge \approx (23,\ 25,\ 26.3,\ 27.9,\ 30.1,\ 33.3), \tag{74}$$
$$100S_\wedge \approx (9.42,\ 10.5,\ 11.3,\ 12.2,\ 13.3,\ 14.8),$$

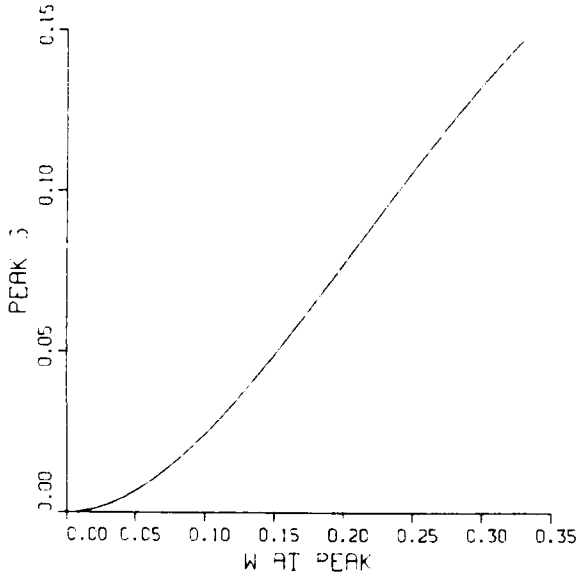

FIG. 10. Peak $S_\wedge$ vs $w_\wedge$ (with c implicit), based on (70), corresponding to Fig. 7.

where the final entries correspond to S_1, as before for (60). The essential aspects of the two sets, and of $S(c;w)$ of (65), change uniformly with c in the range $c \geqslant 0$. (See Appendix for $c < 0$.)

For very large c, we have $w_\wedge \sim 1/\sqrt{3c}$. More generally, we use the complete form in (68), but approximations for c near 1 and 0 are of interest. Thus, for $c \approx 1$,

$$w_\wedge \approx [4 + 3(c-1)/4]^{-1}. \tag{75}$$

At $c = 1$, we obtain the analog of (62),

$$c = 1, \quad w_\wedge = 0.25, \quad S_\wedge \approx 0.105, \quad S = w(1-w)^3. \tag{76}$$

For $c \approx 0$,

$$w_\wedge \approx (1 - c/2 + 5c^2/8)/3 \tag{77}$$

and S reduces to S_1 at $c = 0$.

APPENDIX

For $c < 0$, in terms of $t = c - 1$ and $d = -t > 0$ (for brevity), S is singular at $w_d = 1/d$. In three dimensions, E is nondecreasing and S is non-negative for all w, and we consider the full range for insight. In two dimensions, E decreases and S becomes negative for $w > w_d$, and we restrict consideration to $w < w_d$.

We rewrite the three-dimensional equation of state E of (50) as

$$E = w[1 + w(t-1) + w^2(t^2 - t + 1)/3]/(1-w)^3, \tag{A1}$$

which corresponds to hard convex particles for $t \geqslant 2$. Here, $t = 2$ gives E_3 for spheres, and $t = -1$ gives E_1 for the bound $c = 0$ considered in the text. The first two derivatives with respect to w are

$$E' = \frac{(1+tw)^2}{(1-w)^4} = \frac{1}{W},$$
$$E'' = \frac{2(2+t+tw)(1+tw)}{(1-w)^5} = -\frac{W'}{W^2}. \tag{A2}$$

If $t \geqslant -1$, then E increases monotonically to ∞ as w increases to 1. If $-t = d > 1$ then at $w_d = -1/t = 1/d$ there is a point of inflection ($E' = E'' = 0$) for which $E = w/3(1-w) = 1/3(d-1)$; however (for any real value of t), E cannot vanish for $w > 0$, and is nondecreasing for increasing w. The point of inflection suggests a phase transition, and the corresponding singularity of W and $S = wW$ at w_d suggests the critical region (infinite compressibility ζ).

The fluctuation function

$$S = wW = w(1-w)^4/(1+tw)^2 \tag{A3}$$

is stationary ($S' = 0$) at

$$w_\wedge = \{-(5+t) \pm [(5+t)^2 + 12t]^{1/2}\}/6t. \tag{A4}$$

Both roots are of interest for $t = -d$, as are both values of

$$S''_\wedge = -(1-w)^3(5+t+6tw)/(1+tw)^3, \quad w = w_\wedge. \tag{A5}$$

For all $-t = d > 1$, we see that S is singular at $w_d = 1/d$, and that as w increases past w_d to unity, S decreases monotonically to zero; we therefore need discuss only $w < w_d$. The square root in (A4) vanishes if $-t = d_0 \approx 1.202$; the asso-

ciated stationary point $w_0 = -(5+t)/6t = 2/(5-d_0) \approx 0.5266$ is a point of inflection ($S' = S'' = 0$), after which S increases to ∞ at $w_d = 1/d_0 \approx 0.832$. If $d > d_0$, then (A4) has no real roots, and S increases monotonically from 0 to ∞ as w increases from 0 to w_d. For $1 < d < d_0$, both roots of (A4) correspond to extrema ($w_+ = w_\wedge$, $w_- = w_\vee$) with values satisfying $w_\wedge < w_\vee < w_d = 1/d$. Thus, if $d = 1.2$, then there is a local maximum at $w_\wedge = 1/2$ followed by a local minimum at $w_\vee = 1/1.8$ and a singularity at $w_d = 1/1.2$. If $d = 1.1$, then $w_\wedge \approx 0.38$, $w_\vee \approx 0.81$, and $w_d \approx 0.91$. If d decreases to 1, then $w_\wedge$ decreases to 1/3, and $w_\vee$ and w_d approach 1; in the limit we obtain S_1 as before.

The analogous two-dimensional E of (64) in terms of $t = c - 1$,

$$E = w[2 + (t-1)w]/2(1-w)^2, \tag{A6}$$

corresponds to hard convex disks for $t > 1$. Here, $t = 1$ gives E_2 for circles, and $t = -1$ gives E_1 as for (A1). The first two derivatives with respect to w are

$$E' = (1+tw)/(1-w)^3,$$
$$E'' = (3+t+2tw)/(1-w)^4. \tag{A7}$$

However, although E increases monotonically to ∞ with increasing w for $t > -1$, the behavior for $-t = d > 1$ is quite different than for (A1). The present $w_d = 1/d = -1/t$ (corresponding to $E' = 0$, and E'' negative) represents a local maximum $E = d/2(d-1)^2$; as w increases, E goes to zero at $w = 2/(d+1)$, and then approaches $-\infty$ as $w \to 1$.

The corresponding

$$S = w(1-w)^3/(1+tw) \tag{A8}$$

is stationary at

$$w_\pm = [-2 \pm (4+3t)^{1/2}]/3t, \tag{A9}$$

for which

$$S''_\pm = -(1-w)^2(4+6tw)/(1+tw), \quad w = w_\pm. \tag{A10}$$

For all $-t = d > 1$, we see that S is singular at $w_d = 1/d$, but that in distinction to (A3) the present function changes sign for $w > w_d$ to approach 0 from $-\infty$; we restrict consideration to $w < w_d$. The square root in (A9) vanishes at $-t = d_0 = 4/3$, and $w_0 = 1/2$ is a point of inflection after which S increases to ∞ at $w_d = 3/4$. If $d > 4/3$, then (A9) has no real roots and S increases monotonically from 0 to ∞ as w increases from 0 to w_d. There are two roots for $1 < d < 4/3$; e.g., if $d = 1.2$, then $w_- \approx 0.38$, $w_+ \approx 0.73$, and $w_d \approx 0.83$. If $d \to 1$, then $S \to S_1$ as before.

[1] V. Twersky, "Transparency of pair-correlated random distributions of small scatterers with applications to the cornea," J. Opt. Soc. Am. **65**, 524–530 (1975).

[2] V. Twersky, "Coherent scalar field in pair-correlated random distributions of aligned scatterers," J. Math. Phys. **18**, 2468–2486 (1977).

[3] V. Twersky, "Acoustic bulk parameters in distributions of pair-correlated scatterers," J. Acoust. Soc. Am. **64**, 1710–1719 (1978).

[4] V. Twersky, "Multiple scattering of sound by correlated monolayers," J. Acoust. Soc. Am. **73**, 68–84 (1983); "Reflection and scattering of sound by correlated rough surfaces," J. Acoust. Soc. Am. **73**, 85–94 (1983).

[5] H. L. Frisch and J. L. Lebowitz, *The Equilibrium Theory of Fluids* (Benjamin, New York, 1964).

[6] H. Reiss, H. L. Frisch, and J. L. Lebowitz, "Statistical mechanics of rigid spheres," J. Chem. Phys. **31**, 369–380 (1959); E. Helfand, H. L. Frisch, and J. L. Lebowitz, "The theory of the two- and one-dimensional rigid sphere fluids," J. Chem. Phys. **34**, 1037–1042 (1961).

[7] S. W. Hawley, T. H. Kays, and V. Twersky, "Comparison of distribution functions from scattering data on different sets of spheres," IEEE Trans. Antennas Propag. **AP-15**, 118–135 (1967).

[8] A. Isihara, "Determination of molecular shape by osmotic measurement," J. Chem. Phys. **18**, 1446–1449 (1950); A. Isihara and T. Hayashida, "Theory of high polymer solution," J. Phys. Soc. Jpn. **60**, 40–50 (1951).

[9] H. Hadwiger, *Altes und Neues uber Konvexe Korper* (Birkhauser, Basel, 1955).

[10] T. Kihara, "The second virial coefficient of non-spherical molecules," J. Phys. Soc. Jpn. **6**, 289–296 (1951).

[11] R. M. Gibbons, "The scaled particle theory for particles of arbitrary shape," Mol. Phys. **17**, 81–86 (1969).

[12] A. Isihara, "Theory of high polymer solutions (the dumbbell model)," J. Chem. Phys. **19**, 397–403 (1951).

[13] M. Rigby, "Scaled particle equation of state for hard non-spherical molecules," Mol. Phys. **32**, 575–578 (1976).

[14] J. O. Hirschfelder, C. F. Curtiss, and R. B. Bird, *Molecular Theory of Gases and Liquids* (Wiley, New York, 1954).

[15] K. K. Shung, Y. W. Yuan, D. Y. Fei, and J. M. Tarbell, "Effect of flow disturbance on ultrasonic backscatter from blood," J. Acoust. Soc. Am. **75**, 1265–1272 (1984); Y. W. Yuan and K. K. Shung, "Further studies on ultrasonic backscatter from blood," IEEE Ultrasonics Symp. Proc. (Pub. 84 CH2112-1, IEEE, New York), 666–669 (1984); K. K. Shung, "Physics of blood echogenicity," J. Cardiovas. Ultrasonog. **2**, 401–406 (1983); K. K. Shung, R. A. Sigelmann, and J. M. Reid, "Scattering of ultrasound by blood," IEEE Trans. Biomed. Eng. **BME-23**, 460–467 (1976).

[16] T. Boublik, "Two-dimensional convex particle liquid," Mol. Phys. **29**, 421–428 (1975).

[17] Lord Rayleigh, *Theory of Sound* (Cambridge, 1978; Dover, New York, 1945), Sec. 296 of Dover reprint.

[18] Lord Rayleigh, "On the transmission of light through the atmosphere containing small particles in suspension, and on the origin of the color of the sky," Philos. Mag. **47**, 375–383 (1899).

[19] V. Twersky, "On propagation in random media of discrete scatterers," Proc. Symp. Appl. Math. **16** (AMS, Providence), 84–116 (1965).

[20] H. S. Green, *The Molecular Theory of Fluids* (Interscience, New York, 1952), p. 62ff.

[21] M. S. Wertheim, "Exact solution of the Percus–Yevick integral equation for hard spheres," Phys. Rev. Lett. **10**, 321–323 (1963); E. Thiele, "Equation of state for hard spheres," J. Chem. Phys. **39**, 474–479 (1963).

[22] V. Twersky, "Absorption and multiple scattering by biological suspensions," J. Opt. Soc. Am. **60**, 1084–1093 (1970); see also J. Math. Phys. **3**, 724–734 (1962); J. Opt. Soc. Am. **52**, 145–171 (1962), and J. Acoust. Soc. Am. **36**, 1314–1329 (1964).

[23] V. Twersky, "Propagation in pair correlated distributions of small-spaced lossy scatterers," J. Opt. Soc. Am. **69**, 1567–1572 (1979).